ORIGINAL PAPER

In vivo parameter identification in arteries considering multiple levels of smooth muscle activity

Jan-Lucas Gade[1] · Carl-Johan Thore[1] · Björn Sonesson[2] · Jonas Stålhand[1]

Abstract

In this paper an existing *in vivo* parameter identification method for arteries is extended to account for smooth muscle activity. Within this method a continuum-mechanical model, whose parameters relate to the mechanical properties of the artery, is fit to clinical data by solving a minimization problem. Including smooth muscle activity in the model increases the number of parameters. This may lead to overparameterization, implying that several parameter combinations solve the minimization problem equally well and it is therefore not possible to determine which set of parameters represents the mechanical properties of the artery best. To prevent overparameterization the model is fit to clinical data measured at different levels of smooth muscle activity. Three conditions are considered for the human abdominal aorta: basal during rest; constricted, induced by lower-body negative pressure; and dilated, induced by physical exercise. By fitting the model to these three arterial conditions simultaneously a unique set of model parameters is identified and the model prediction agrees well with the clinical data.

Keywords *In vivo* · Parameter identification · Artery · Smooth muscle activity

1 Introduction

Cardiovascular diseases are the leading cause of death in the western world (Mozaffarian et al. 2016; Wilkins et al. 2017). People at risk of developing cardiovascular diseases are generally found by evaluating a risk score which comprises several biomarkers such as age, sex, blood pressure, etc. (Vlachopoulos et al. 2015; Curry et al. 2018). Risk scores are, however, not flawless, and there is a constant search for better ways to assess the risk for cardiovascular disease development. One risk marker, which has attracted a lot of attention in recent years, is arterial stiffness (Laurent et al. 2012; Van Sloten et al. 2014).

Arterial stiffness reflects the mechanical properties of the arterial wall as a whole, and its constituents and their arrangement in particular. From a mechanical point of view, elastin, collagen and smooth muscle cells are the most important wall constituents (Holzapfel et al. 2000). While elastin and collagen build up an extracellular network providing passive structural integrity to the arterial wall, the embedded smooth muscle cells modulate arterial stiffness through their ability to actively contract or relax in the short term and by synthesis of new extracellular matrix proteins in the long term (Rhodin 2014). The ability to actively change arterial stiffness within seconds is not only essential for vital blood flow circulation but also helps to counteract negative effects of cardiovascular diseases and their development. During early hypertension an increased vasoactivity stiffens the arterial wall which returns the transmural stress gradient back to its normotensive value (Fridez et al. 2002; Sehgel et al. 2013; Humphrey and Wilson 2003). With sustained hypertension the arterial wall adapts slowly by growth and remodeling and the vasoactivity returns back to baseline values (Matsumoto and Hayashi 1996; Fridez et al. 2002).

Several measures have been introduced to assess arterial stiffness in the clinic. The most prominent one is to determine the pulse wave velocity between the carotid and the femoral artery (Bramwell and Hill 1922). This noninvasive method is simple to use but averages the arterial stiffness over the aorta and assumes a constant stiffness despite the distinctive nonlinear stiffening behavior of the arterial wall (Roach and Burton 1957). Other popular measures

✉ Jan-Lucas Gade
jan-lucas.gade@liu.se

1 Department of Management and Engineering, Division of Solid Mechanics, Linköping University, Linköping, Sweden

2 Department of Cardiothoracic and Vascular Surgery, Skåne University Hospital, Malmö, Sweden

such as the pressure-strain elastic modulus E_p (Peterson et al. 1960) and the stiffness index β (Kawasaki et al. 1987) suffer similar limitations. Furthermore, all of these arterial stiffness measures are blood-pressure dependent (Zieff et al. 2019) and do not distinguish between arterial wall constituents.

To address these shortcomings several research groups have proposed methods that use continuum-based mechanical models whose parameters are related to the stiffness of the arterial wall constituents (Masson et al. 2008; Spronck et al. 2015; Smoljkić et al. 2015; Wittek et al. 2016; Heusinkveld et al. 2018; Gade et al. 2019; Schulze-Bauer and Holzapfel 2003). The model parameters are identified by fitting the model's response to clinical measurements which typically comprise time-resolved pressure-radius pairs and information about the cross-sectional wall area. Information about the *in situ* axial prestretch, axial force, perivascular support, the stress-free reference configuration, and the level of smooth muscle activity is missing, however. This limited amount of *in vivo* obtainable data restricts the number of model parameters which can be uniquely identified (Stålhand and Klarbring 2005; Reesink and Spronck 2019). Introducing too many model parameters leads to overparameterization, meaning that a (nonlinear) parameter combination can be continuously changed without affecting the objective function value. This makes it impossible to determine which set of parameters represents the mechanical properties of the artery. To prevent overparameterization the complexity of the continuum-mechanical models is reduced and a common simplification concerning smooth muscle activity is to either neglect it (Smoljkić et al. 2015; Wittek et al. 2016; Heusinkveld et al. 2018; Gade et al. 2019; Schulze-Bauer and Holzapfel 2003) or to account for it but fix some model parameters to values reported in the literature (Spronck et al. 2015). An exception is the method proposed in Masson et al. (2008). Their model requires 14 parameters to be identified, however, making it very questionable whether a unique solution has been obtained (Spronck et al. 2015).

It was hypothesized in Reesink and Spronck (2019) that smooth muscle activity can be included without causing overparameterization if the arterial model is fit to multiple *in vivo* data sets collected at different levels of vascular tone. To the best of the author's knowledge this idea has not been implemented yet. In this paper we therefore extend the mechanical model in Gade et al. (2019) to account for smooth muscle activity and fit the model to *in vivo* data sets collected at rest and while the artery was in a constricted and a dilated condition.

The paper is structured as follows. First the mechanical model from Gade et al. (2019) is described and extended to account for smooth muscle activity. Afterward the fitting procedure by means of solving a multi-objective minimization problem is discussed. The material used in this study is introduced next, followed by the results section. The paper is concluded with a discussion and a final conclusion.

2 Mechanical model for arteries

The mechanical model in Gade et al. (2019) treats an artery as a homogeneous, incompressible, residual stress-free, thin-walled cylinder. *Ex vivo* in the absence of external loads, the artery has an inner radius R_i, wall thickness H, and a length L. This state is taken to be the stress-free reference configuration. *In situ* the artery is stretched to a length l, which is taken to be constant throughout the cardiac cycle (Van Loon et al. 1977; Weizsäcker et al. 1983), and the inner radius and wall thickness are denoted r_i and h, respectively. In this deformed configuration, the artery is exposed to the blood pressure P and an axial force, where the latter cannot be measured *in vivo*. A consequence of incompressibility in combination with the constant length l is that the deformed cross-sectional area $A = 2\pi r_i h + \pi h^2$ is constant.

In the deformed configuration two sets of stresses are calculated for an artery: equilibrium stresses depending on the *in vivo* data and the unknown axial force; and constitutively determined stresses depending also on the model parameters to be identified.

2.1 Equilibrium stresses

By stating global equilibrium in the deformed configuration, the arterial stress state reduces to a principal stress state with components in the circumferential, axial and radial direction, i.e., Laplace laws. The circumferential and axial stress are

$$\sigma_{\theta\theta}^{Lp} = \frac{Pr_i}{h} \tag{1}$$

and

$$\sigma_{zz}^{Lp} = \frac{\pi r_i^2 P + \bar{F}_{red}}{\pi h (2r_i + h)}, \tag{2}$$

respectively. The radial stress is assumed to be zero due to the thin-walled assumption, i.e., $\sigma_{rr}^{Lp} = 0$. The axial force $\bar{F}_{red}$ in Eq. (2), also referred to as the reduced axial force (Holzapfel et al. 2000), is reported to be approximately constant at the *in situ* axial prestretch in the physiological pressure range (Van Loon et al. 1977; Weizsäcker et al. 1983). The magnitude of $\bar{F}_{red}$ is unknown and was estimated in Gade et al. (2019) since it could not be uniquely identified from a single *in vivo* data set.

2.2 Constitutively determined stresses

In order to determine the arterial stress state constitutively the kinematic relationship is needed. Using the cylindrical base vectors $\mathbf{e}_\theta$, $\mathbf{e}_z$, and $\mathbf{e}_r$ the deformation gradient $\mathbf{F}$ describing the deformation out of the reference configuration into the deformed configuration becomes

$$\mathbf{F} = \lambda_\theta \mathbf{e}_\theta \otimes \mathbf{e}_\theta + \lambda_z \mathbf{e}_z \otimes \mathbf{e}_z + \lambda_r \mathbf{e}_r \otimes \mathbf{e}_r, \tag{3}$$

where λ_θ, λ_z, and λ_r are the three principal stretches. The three stretches must satisfy the constraint

$$\det \mathbf{F} = \lambda_\theta \lambda_z \lambda_r = 1 \tag{4}$$

to comply with the assumed incompressible behavior and, therefore, only two stretches can be independently determined. The circumferential stretch is defined in the mid-wall as

$$\lambda_\theta = \frac{2r_\mathrm{i} + h}{R_\mathrm{i} + \sqrt{R_\mathrm{i}^2 + \lambda_z h \left(2r_\mathrm{i} + h\right)}}, \tag{5}$$

where the axial stretch is taken as an independent variable. The radial stretch is implicitly given by Eq. (4) (Gade et al. 2019).

The behavior of the arterial wall is additively split into two parts: a passive and an active part (Hill 1938). The passive response of the arterial wall is derived from a strain energy density function Ψ describing the (passive) interaction of fibers and cells. The active part $\boldsymbol{\sigma}^\mathrm{act}$ is associated with the (active) contraction of smooth muscle cells. The constitutive equation in terms of the Cauchy stress tensor $\boldsymbol{\sigma}$ thus reads

$$\boldsymbol{\sigma}^\mathrm{mod} = -p\mathbf{I} + 2\mathbf{F}\frac{\partial \Psi}{\partial \mathbf{C}}\mathbf{F}^\mathrm{T} + \boldsymbol{\sigma}^\mathrm{act}, \tag{6}$$

where the superscript mod denotes model, p is a Lagrange multiplier arising from the incompressibility constraint in Eq. (4), $\mathbf{I}$ denotes the second-order identity tensor, and $\mathbf{C} = \mathbf{F}^\mathrm{T}\mathbf{F}$ is the right Cauchy-Green stretch tensor.

The Lagrange multiplier p can be calculated from the radial component in Eq. (6) by taking $\sigma_{rr} = 0$, cf. Section 2.1. The specific forms of Ψ and $\boldsymbol{\sigma}^\mathrm{act}$ are introduced in the following sections.

2.2.1 Passive arterial response

The passive behavior of the arterial wall is modeled using the HGO strain energy density function Ψ (Holzapfel et al. 2000). This strain energy is additively decomposed into an isotropic part Ψ_iso and an anisotropic part Ψ_aniso. The isotropic part is associated with noncollagenous matrix material

such as elastin and is taken as the classical neo-Hookean model (Treloar 1943)

$$\Psi_\mathrm{iso} = c\left(I_1 - 3\right), \tag{7}$$

where $c > 0$ and $I_1 = \mathrm{tr}\,\mathbf{C}$. The anisotropic part is associated with the embedded collagen fibers which are assumed to belong to one of two mechanically equivalent fiber families oriented along the referential unit vectors $\mathbf{M}$ and $\mathbf{N}$. Both fiber families are assumed to be symmetrically arranged around the circumferential direction with the pitch angle $\pm\beta$ in the reference configuration, so

$$\mathbf{M} = \cos\beta\,\mathbf{e}_\theta + \sin\beta\,\mathbf{e}_z, \quad \mathbf{N} = \cos\beta\,\mathbf{e}_\theta - \sin\beta\,\mathbf{e}_z. \tag{8}$$

The strain energy of the fiber families is given by

$$\Psi_\mathrm{aniso} = \frac{k_1}{2\,k_2}\left(e^{k_2\left(I_4 - 1\right)^2} + e^{k_2\left(I_6 - 1\right)^2} - 2\right), \tag{9}$$

where

$$I_4 = \mathbf{M} \cdot \mathbf{CM}, \quad I_6 = \mathbf{N} \cdot \mathbf{CN}, \tag{10}$$

and $k_1, k_2 > 0$. The pseudo-invariants I_4 and I_6 are equal to the squared stretch along each fiber family, and using Eqs. (3), (8), and (10), it holds that

$$I_4 = I_6 = \lambda_\theta^2 \cos^2\beta + \lambda_z^2 \sin^2\beta. \tag{11}$$

The collagen fibers are assumed to only support tensile loads and buckle in compression (Holzapfel et al. 2000). The anisotropic contribution Ψ_aniso is, therefore, omitted from Ψ if $I_4, I_6 < 1$.

2.2.2 Active arterial response

The ability of an artery to actively constrict and dilate the lumen by changing the contracted state of the smooth muscle cells inside the wall gives rise to an active stress $\boldsymbol{\sigma}^\mathrm{act}$. Smooth muscle cells are reported to be primarily oriented in the circumferential direction (Dobrin 2011; Rhodin 2014), and following Rachev and Hayashi (1999) we take

$$\boldsymbol{\sigma}^\mathrm{act} = S\lambda_\theta f \mathbf{e}_\theta \otimes \mathbf{e}_\theta, \tag{12}$$

where S is the generated isometric stress (per unit reference area) related to the level of smooth muscle activation, and f is a function accounting for the parabolic length–tension relationship of smooth muscle (Price et al. 1981; Cox 1978; Dobrin 1973) which satisfies $\max f = 1$. Smooth muscle cells are reported to contract slowly, on the order of ten seconds or more until peak tension, but are able to maintain this state for long periods of time (Somlyo and Somlyo 1992; Dobrin 2011). We, therefore, consider vascular smooth muscle cells to contract at mean arterial blood pressure (MAP) and keep

this state until the mechanical and/or chemical environment changes. Accordingly we evaluate the length–tension relationship at MAP and take

$$f = f\left(\lambda_\theta^{\text{MAP}}\right) = \exp\left[-\frac{\left(\lambda_\theta^{\text{opt}} - \lambda_\theta^{\text{MAP}}\right)^2}{2\omega^2}\right], \tag{13}$$

where $\lambda_\theta^{\text{opt}} = 1.4$ is the optimal stretch for maximum force generation (Rachev and Hayashi 1999) and $\omega = 0.45$ controls the width of the parabola-like exponential function. The value for ω is chosen such that the length–tension relationship in Eq. (13) resembles the parabola suggested in Rachev and Hayashi (1999) well in the relevant interval given by $0.8 \leq \lambda_\theta \leq 1.4$.

3 Parameter identification method

Let a pressure-radius data set consisting of blood-pressure and inner-radius pairs $\left(P_{qj}, r_{\text{i},qj}\right)$ at $j = 1, \ldots, n$ time points for arterial condition $q = 1$ (basal), 2 (constricted), 3 (dilated) be given together with information about the cross-sectional area A. The equilibrium and constitutively determined stresses in Sect. 2 are then defined down to, respectively, the reduced axial force $\bar{F}_{\text{red}}$ and the model parameters: R_{i}, λ_z, c, k_1, k_2, β, and S_q. The last parameter S_q is the isometric stress for arterial condition q. Note that the model parameters associated with the deformation $\left(R_{\text{i}}, \lambda_z\right)$ and the passive material $\left(c, k_1, k_2, \beta\right)$ do not depend on the arterial condition.

All model parameters are identified by minimizing a normalized sum of the weighted least-squares differences between the equilibrium and constitutively determined stresses for each arterial condition. The weighted least-squares difference for arterial condition q is defined as

$$\varepsilon_q(\kappa, \bar{F}_{\text{red}}, S_q) = \sum_{j=1}^{n} \left\{ w_q \left[\sigma_{\theta\theta}^{\text{mod}}(\kappa, S_q, r_{\text{i},qj}) \right. \right.$$
$$\left. - \sigma_{\theta\theta}^{\text{Lp}}(r_{\text{i},qj}, P_{qj})\right]^2 + (1 - w_q)$$
$$\left. \left[\sigma_{zz}^{\text{mod}}(\kappa, r_{\text{i},qj}) - \sigma_{zz}^{\text{Lp}}(r_{\text{i},qj}, P_{qj}, \bar{F}_{\text{red}})\right]^2 \right\} \tag{14}$$

where $\kappa = \left(R_{\text{i}}, \lambda_z, c, k_1, k_2, \beta\right)$. The weighting factors for the three conditions are $w_1 = 0.5$ and $w_2 = w_3 = 1.0$. Hence, the axial part of the individual objective ε_q is only considered for the basal condition justifying the use of a single reduced axial force instead of one for each arterial condition. Furthermore, the closer a weighting factor is to zero, the more the axial part will dominate the individual objective and as a consequence the deviation of the constitutive model's response from a constant reduced axial force with magnitude $\bar{F}_{\text{red}}$ is penalized, see Discussion. By choosing $w_1 = 0.5$, an approximately constant reduced axial force is obtained for

the basal condition while still achieving a high agreement in the circumferential direction.

The parameter identification for a given subject is done for the three arterial conditions simultaneously, making it a multi-objective minimization problem with the individual objectives ε_q. One way to handle it numerically is to minimize a weighted sum of the individual objectives, thus reducing the problem to a single-objective minimization problem. This approach is greatly affected by the magnitude of the individual objectives relative to each other and some form of normalization is typically needed. Without normalization the arterial condition with the highest objective function value dominates the parameter identification and the resulting best-fit parameters would only represent this condition well. Here we adopt a normalization scheme based on so-called Utopia and Nadir points to provide equal weight to each arterial condition (Mausser 2006).

The normalized sum of the individual objectives is

$$\varepsilon(\kappa, \bar{F}_{\text{red}}, S) = \sum_{q=1}^{3} \frac{\varepsilon_q(\kappa, \bar{F}_{\text{red}}, S_q) - \varepsilon_q^{\text{Utopia}}}{\varepsilon_q^{\text{Nadir}} - \varepsilon_q^{\text{Utopia}}}, \tag{15}$$

where $S = \left(S_1, S_2, S_3\right)$ and $\varepsilon_q^{\text{Utopia}}$ and $\varepsilon_q^{\text{Nadir}}$ are the Utopia and Nadir point for condition q, respectively.

The Utopia point is the lowest least-squares difference if only arterial condition q is considered, i.e., the objective function value when minimizing Eq. (14). The corresponding minimization problem is, however, overparameterized, and no unique solution for the parameter vector $\left(\kappa, \bar{F}_{\text{red}}, S_q\right)$ is obtained. Instead, the closely related (Utopia) minimization problem is solved:

$$\left(\mathbb{U}_q\right) \begin{cases} \underset{\kappa \in \mathbb{R}^6}{\text{minimize}} & \hat{\varepsilon}_q(\kappa, 1, 0) \\ \text{subject to:} & \kappa^{\text{min}} \leq \kappa \leq \kappa^{\text{max}}, \end{cases}$$

where the superscripts min and max denote lower and upper bound, respectively, and $\hat{\varepsilon}_q$ is given by Eq. (14) with w_q set to 0.99. Hence, a completely passive arterial behavior, i.e., $S_q = 0$, is assumed and a reduced axial force of 1 N in combination with a weighting factor of 0.99 is used for every condition to stabilize the minimization. The unique parameter vector κ_q^* that minimizes $\left(\mathbb{U}_q\right)$ is then used to calculate the Utopia point, i.e., $\varepsilon_q^{\text{Utopia}} = \varepsilon_q(\kappa_q^*, 1, 0)$.

The Nadir point of condition q is the least-squares difference when the parameter vector of another Utopia point is used to evaluate ε_q. Hence, the Nadir point of condition $q = 1$ (basal) is

$$\varepsilon_1^{\text{Nadir}} = \max\left[\varepsilon_1(\kappa_2^*, 1, 0), \varepsilon_1(\kappa_3^*, 1, 0)\right]. \tag{16}$$

The Utopia and Nadir points are best-case and worst-case values, and it is easy to see that in Eq. (15), each individual objective is bounded by

Table 1 Fitting ranges for the parameter identification (Horný et al. 2011, 2014; Ferruzzi et al. 2011; Gade et al. 2019; Rachev and Hayashi 1999; Schulze-Bauer et al. 2003)

Parameter	Unit	Min	Max
R_i	[mm]	1	20
λ_z	[−]	1	1.5
c	[kPa]	0.0001	1000
k_1	[kPa]	0.0001	1000
k_2	[−]	0.0001	1000
β	[deg]	0	90
$\bar{F}_{red}$	[N]	0	1.5
S	[kPa]	0	150

$$0 \lesssim \frac{\varepsilon_q(\boldsymbol{\kappa}, \bar{F}_{red}, S_q) - \varepsilon_q^{\text{Utopia}}}{\varepsilon_q^{\text{Nadir}} - \varepsilon_q^{\text{Utopia}}} \lesssim 1, \tag{17}$$

providing equal weight to each pressure-radius loop. Note that the lower and upper bounds in Eq. (17) are only approximate due to the Utopia and Nadir point calculation, see Discussion.

The complete parameter identification problem reads:

$$(\mathbb{P}) \begin{cases} \underset{(\boldsymbol{\kappa}, \bar{F}_{red}, \boldsymbol{S}) \in \mathbb{R}^{10}}{\text{minimize}} & \varepsilon(\boldsymbol{\kappa}, \bar{F}_{red}, \boldsymbol{S}) \\ \text{subject to:} & \begin{cases} \boldsymbol{\kappa}^{\min} \leq \boldsymbol{\kappa} \leq \boldsymbol{\kappa}^{\max}, \\ \bar{F}_{red}^{\min} \leq \bar{F}_{red} \leq \bar{F}_{red}^{\max}, \\ \boldsymbol{S}^{\min} \leq \boldsymbol{S} \leq \boldsymbol{S}^{\max}. \end{cases} \end{cases}$$

The fitting ranges for the model parameters are motivated by experimental observations but adjusted so that they do not become active when solving ($\mathbb{P}$)), see Table 1. The lower limit for λ_z is set to 1.0 to prevent buckling because this phenomenon is not considered in the mechanical model.

3.1 Implementation

The parameter identification problem ($\mathbb{P}$) and the Utopia problems ($\mathbb{U}_q$) are nonlinear and nonconvex. Such problems generally possess local solutions which are not global solutions (Nocedal and Wright 1999). We, therefore, adopt the heuristic method used in Gade et al. (2019): (i) solve ($\mathbb{P}$) and ($\mathbb{U}_q$) using 100 starting points generated using Latin Hypercube sampling and take the solution with the lowest objective function value as the global solution; (ii) use the analytical gradient and Hessian of Eq. (15); (iii) and make ($\mathbb{P}$) and ($\mathbb{U}_q$) more balanced by replacing c, k_1, k_2 and β by scaled counterparts according to

$$c = e^{\tilde{c}}, \quad k_1 = e^{\tilde{k}_1}, \quad k_2 = e^{\tilde{k}_2}, \quad \beta = \arcsin\sqrt{\tilde{\beta}}. \tag{18}$$

The minimization problems are solved in MATLAB R2019b (The MathWorks Inc., Natick, MA, USA). A *MultiStart* class is defined to solve the minimization problems from the generated starting points using the *interior-point* optimization algorithm of the function *fmincon*. The analytical gradient and Hessian of Eq. (15) are determined with MAPLE 2015.1 (Maplesoft, Waterloo, Ontario) and supplied to *fmincon*.

A minimal working example of the parameter identification method is found in the supplementary material.

4 Material

The material for this study is taken from Sonesson et al. (1997) and comes from the abdominal aorta of two healthy, non-smoking Caucasian females. Subjects I and II are 24 and 26 years of age, respectively. The blood pressure and inner radius were measured simultaneously in the supine position using a catheter (invasive) and an echo-tracking system (noninvasive), respectively. Figure 1 shows the measurement
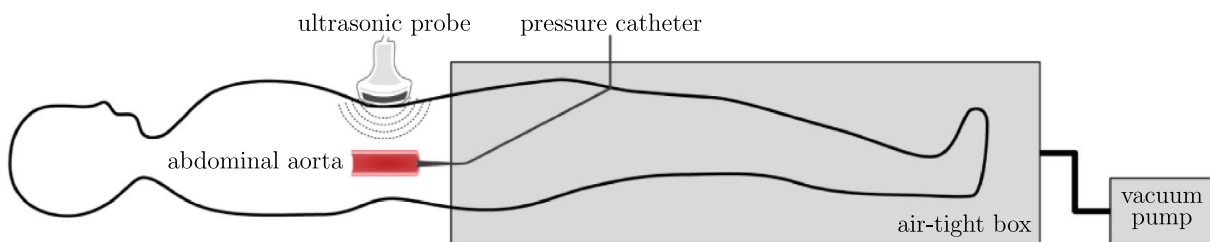

Fig. 1 Schematic drawing of the experimental setup for simultaneous measurement of blood pressure and inner radius in the abdominal aorta during rest, lower-body negative pressure, and physical exercise

setup, and for more details about the data acquisition, the reader is referred to the original paper and Sonesson et al. (1994). Besides performing the measurements at rest, Sonesson et al. (1997) collected pressure and radius data while the aorta was in a constricted and a dilated condition[1]. The constricted condition was obtained by placing the subject's lower body in a hermetically sealed chamber and reducing the pressure inside to near vacuum. This lower-body negative pressure technique causes pooling of blood in the lower extremities resulting in vasoconstriction (Vukasovic et al. 1990; White et al. 1996). The dilated condition was achieved by physical exercise (Green et al. 2017; MacDougall 1994) by means of asking the subject to clench their fists four times. The study was approved by the Ethics Committee at Lund University, Sweden, and all subjects gave informed consent.

The raw measurements are reduced to two to seven pressure-radius loops once the abdominal aorta has reached a stable state in the respective condition. From this data pressure-radius loops consisting of $n = 100$ equidistant data points are created for each subject and aortic condition following Stålhand (2009). The pressure-radius loops for subjects I and II are presented in Figs. 2 and 3, respectively.

For each pressure-radius loop, MAP is calculated according to Tortora and Derrickson (2012)

$$P^{\mathrm{MAP}} = P^{\mathrm{dia}} + \frac{1}{3}\left(P^{\mathrm{sys}} - P^{\mathrm{dia}}\right), \tag{19}$$

where P^{dia} and P^{sys} are the diastolic and systolic blood pressure, respectively.

Neither the deformed wall thickness nor the deformed wall cross-sectional area were recorded in Sonesson et al. (1997). The deformed wall cross-sectional area is, therefore, estimated as $A = 20.52 + 0.58 \cdot \mathrm{age}$, where A is in mm^2 and age is in years (Åstrand et al. 2011). The equation has been determined by evaluating the age-dependent increase of the intima-media area in the female abdominal aorta provided in Åstrand et al. (2005) and the assumption that the adventitia comprises one-third of the arterial wall (Holzapfel et al. 2007). The cross-sectional areas are accordingly estimated to $34.44\ \mathrm{mm}^2$ and $35.60\ \mathrm{mm}^2$ for subjects I and II, respectively.

5 Results

For both subjects I and II, three pressure-radius loops measured at different levels of vascular tone are available, see Sect. 4. Hence, three levels of smooth muscle activation are included in the parameter identification and ten parameters are identified for each subject. Solving the minimization problems took less than 2 min on a hexa-core 2.9 GHz CPU

---

[1] The measurements in the dilated condition were not published in Sonesson et al. (1997).

Table 2 Identified parameters for subjects I and II

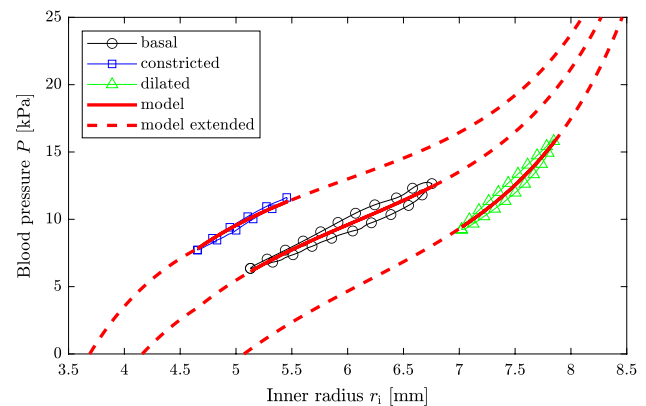| Parameter	Unit	Subject I	Subject II
R_{i}	[mm]	5.99	6.69
λ_z	[–]	1.32	1.15
c	[kPa]	22.51	54.59
k_1	[kPa]	25.79	52.22
k_2	[–]	1.72	7.50
β	[deg]	35.27	37.58
$\bar{F}_{\mathrm{red}}$	[N]	1.18	1.28
S_{basal}	[kPa]	61.19	55.58
$S_{\mathrm{constricted}}$	[kPa]	136.80	93.56
S_{dilated}	[kPa]	< 0.01	28.37

Fig. 2 Measured pressure-radius loops and model predictions for subject I. The solid red lines are the model predictions of the three arterial conditions considered within the parameter identification. The arterial behavior outside the measured pressure-range is predicted and shown as the dashed red lines for each condition
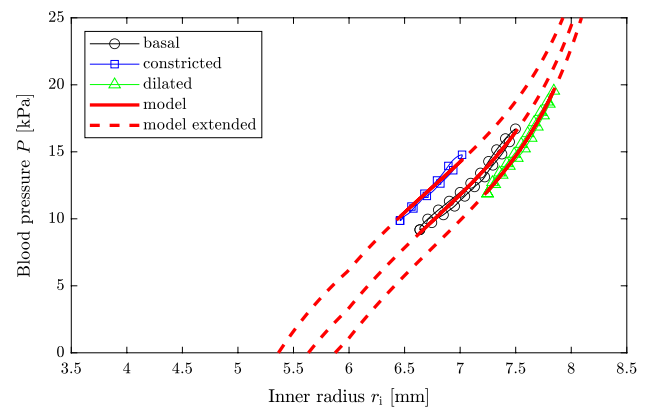

Fig. 3 Measured pressure-radius loops and model predictions for subject II. The solid red lines are the model predictions of the three arterial conditions considered within the parameter identification. The arterial behavior outside the measured pressure-range is predicted and shown as the dashed red lines for each condition

and at least 70% of all starting points converged to the same solution with the lowest objective function value for each subject. The identified model parameters are summarized in Table 2. Additional details about the Utopia and Nadir points are provided in the supplementary material.

In order to compare the measured pressure-radius data and the identified reduced axial force with the model prediction, the model blood pressure P^{mod} and the model reduced axial force $F_{\mathrm{red}}^{\mathrm{mod}}$ are introduced. These two quantities are calculated by replacing the Laplace stresses in Eqs. (1) and (2) with the constitutively determined stresses given by Eqs. (3), (5), (6), (7), (9), (11), (12), and (13), as

$$P^{\mathrm{mod}} = \sigma_{\theta\theta}^{\mathrm{mod}} \frac{h}{r_{\mathrm{i}}} \tag{20}$$

and

$$F_{\mathrm{red}}^{\mathrm{mod}} = \sigma_{zz}^{\mathrm{mod}} \pi h \left(2r_{\mathrm{i}} + h\right) - \pi r_{\mathrm{i}}^2 P^{\mathrm{mod}}. \tag{21}$$

Figures 2 and 3 show the comparison of the measured pressure-radius loops and the model predictions for subjects I and II, respectively. In order to quantify the agreement between the predicted and the measured pressure-radius loops, Table 3 displays for each arterial condition the coefficient of determination (Nash and Sutcliffe 1970)

$$R_q^2 = 1 - \frac{\sum\limits_{j=1}^{n} \left(P_{qj} - P_{qj}^{\mathrm{mod}}\right)^2}{\sum\limits_{j=1}^{n} \left(P_{qj} - \bar{P}_q\right)^2}, \tag{22}$$

where $\bar{P}_q$ is the mean of P_{qj}. To further put the agreement into perspective, Table 3 also contains the coefficient of determination in case the model parameters are identified for each arterial condition individually, as when computing the Utopia point in Sect. 3.

In Fig. 4, the arterial models behavior in terms of the reduced axial force is displayed for both subjects. As can be seen, the predicted reduced axial force is approximately constant in the basal condition for both subjects.

6 Discussion

In this study the possibility to account for smooth muscle activity in a continuum-mechanical model is evaluated. To prevent overparameterizaton the model is fit simultaneously to three pressure-radius loops measured at different levels of smooth muscle activity. Although pressure-radius data are available in the basal, constricted and dilated condition for 19 subjects, only two young females are included in this study. The reason for this limitation is the necessity to fit
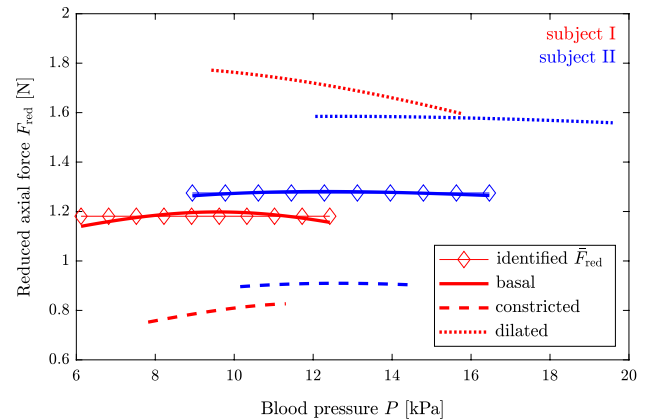

Fig. 4 Identified reduced axial force and model prediction for both subjects. The colors red and blue are used for subjects I and II, respectively

Table 3 Agreement of the measured pressure-radius loops and the model predictions in terms of $R^2 \in (-\infty, 1]$, where 1 represents a perfect fit. The column denoted 'combined' represents the case when the model parameters are identified considering all arterial conditions, cf. Table 2. The column 'individual' represents the case when the model parameters are identified using only the respective arterial condition, as when computing the Utopia point in Sect. 3

	Condition	Combined R^2	Individual R^2
Subject I	Basal	0.94	0.94
	Constricted	0.96	0.97
	Dilated	0.94	0.94
Subject II	Basal	0.97	0.98
	Constricted	0.96	0.97
	Dilated	0.98	0.98

the mechanical model to all three arterial conditions simultaneously. If only two conditions are considered, e.g., basal and constricted, the parameter combination can be continuously changed without affecting the objective function value, indicating that the problem is overparameterized, see supplementary material for an example. The resting and constricted arterial conditions give stable pressure-radius loops over consecutive cardiac cycles. In contrast, the physical exercise frequently caused unstable pressure-radius loops possibly due to varying smooth muscle tone or measurement errors such as involuntary motion of the ultrasonic probe. Furthermore, the pressure-radius measurements during rest and lower-body negative pressure were repeated and we only

Table 4 Generated active stress σ^{act} and total circumferential stress $\sigma_{\theta\theta}$ at MAP

	Condition	σ^{act} [kPa]	$\sigma_{\theta\theta}$ [kPa]
Subject I	Basal	32.93	51.72
	Constricted	49.15	42.72
	Dilated	< 0.01	111.66
Subject II	Basal	40.66	103.98
	Constricted	60.20	94.68
	Dilated	24.60	145.06

consider subjects whose repeated measurements agree[2]. Unfortunately it was only for the two included subjects that the data of all three arterial conditions contained stable pressure-radius loops over consecutive cardiac cycles and whose repeated measurements agreed with each other. In a future study it is, therefore, recommended to induce the dilated state by, e.g., pharmacological intervention (Boutouyrie et al. 2011) or the isometric handgrip exercise (Atkinson et al. 2015) to create a more stable pressure-radius response.

The proposed mechanical model in combination with the minimization scheme satisfactorily fits the measured pressure-radius loops at multiple levels of arterial tone, see Figs. 2 and 3, and the reduced axial force is reasonably constant in the basal condition, see Fig. 4. Additional figures showing the circumferential and axial stress as a function of the circumferential stretch are found in the supplementary material for both subjects.

The identified parameters for the passive part of the arterial wall are in the same range as what has been reported previously for the human abdominal aorta (Horný et al. 2011, 2014; Ferruzzi et al. 2011; Schriefl et al. 2012; Gade et al. 2019). Only the identified axial prestretch of subject II is slightly lower than what is to be expected for a 26-year-old (Horný et al. 2011). However, the deformed inner radius is quite large for subject II and the basal pressure-radius loop agrees better with the middle-aged population (Sonesson et al. 1994) which may explain the discrepancy.

To the best of the author's knowledge, no information about the reduced axial force of the abdominal aorta in young females has been published. The identified forces have, however, a similar magnitude compared to the abdominal aorta of older subjects (Gade et al. 2019), the human thoracic aorta (Schulze-Bauer and Holzapfel 2003), and aged human iliac arteries (Schulze-Bauer et al. 2003).

The identified smooth muscle activations agree nicely with the levels suggested for basal muscular tone under normal physiological conditions, $S = 50$ kPa, and maximal contraction, $S = 100$ kPa, in case of subject II (Rachev and Hayashi 1999). For subject I, the calculated values are higher, especially under maximal contraction, cf. $S_{\mathrm{constr.}} = 136.80$ kPa in Table 2. Despite the apparent higher smooth muscle activation for subject I, the generated active stress is instead larger for subject II, cf. Table 4. This is related to the length–tension relationship which is only $f\left(\lambda_{\theta,\mathrm{constr.}}^{\mathrm{MAP}}\right) = 0.44$ for subject I but 0.65 for subject II. This suggests that the smooth muscle cells are at a more contraction efficient length for subject II. With respect to the dilated arterial condition, it appears that clenching the fist four times resulted in a complete relaxation of smooth muscle cells for subject I, but created a much smaller response for subject II. This behavior is expressed in Figs. 2 and 3 where the pressure-radius loop in the dilated state is shifted substantially to higher radii for subject I but barely changed for subject II.

The values of the smooth muscle activation must, however, be interpreted with caution. The active stress depends on the product Sf. If the length–tension relationship is changed, the identification would result in a different smooth muscle activation such that the product remains constant. It is therefore difficult to compare the identified smooth muscle activation with other studies besides Rachev and Hayashi (1999). This is particularly true if a different smooth muscle model is used (Zulliger et al. 2004; Spronck et al. 2015).

The generated active stress at MAP during the three arterial conditions is summarized in Table 4 for both subjects. To the best of the author's knowledge this is the first study that presents *in vivo* stress values resulting from smooth muscle contraction for the human abdominal aorta. Compared to other arteries and other species, the values reported herein are in the same range (Dobrin 1978; Murtada et al. 2012; Cox et al. 1976). According to Table 4 the active stress accounts for a considerable part of the total stress in the circumferential direction already in the resting condition. This suggests that even for the elastic abdominal aorta, smooth muscle tonus is important and should be accounted for.

Figures 2 and 3 unequivocally show that the human abdominal aorta can modulate its stiffness by altering smooth muscle tonus. This is especially pronounced for subject I for which not only the deformation reduces with smooth muscle contraction but also the shape of the pressure-radius loop changes substantially. While the deformation of the dilated condition is primarily governed by collagen, a shift toward the isotropic matrix is visual in the basal and constricted conditions, see Fig. 2. In order to illustrate the effect of smooth muscle contraction on

---

[2] One measurement was performed during the physical exercise and another one directly afterward. Due to the dynamic nature of the exercise only the latter measurement contained stable pressure-radius loops.

Table 5 Arterial stiffness in terms the pressure-strain elastic modulus E_p and the stiffness index β

	Condition	E_p [kPa]	$\beta[-]$
Subject I	Basal	20.21	5.86
	Constricted	22.63	7.89
	Dilated	57.11	16.16
Subject II	Basal	58.03	15.56
	Constricted	56.74	18.37
	Dilated	92.91	24.69

arterial deformation behavior even further, the arterial model together with the identified parameters is used to predict the aortic behavior outside the physiological range for each degree of smooth muscle activation. This behavior is illustrated as the dashed red lines in Figs. 2 and 3. As one can see, the effect of smooth muscle activity is largest for low blood pressure and with increasing deformation, the three curves approach each other.

The statement that the abdominal aorta can modulate its stiffness stands in contrast to Sonesson et al. (1997) who used the same data set but concluded that the stiffness is unaffected by the sympathetic reaction due to lower-body negative pressure. Although Sonesson et al. (1997) based their conclusion on evaluating 19 subjects, compared to the two out of the 19 in this study, they assessed arterial stiffness in terms of E_p, β and pressure change-in-diameter curves. The stiffness measures E_p and β describe the average slope of the pressure-radius relationship. As can be seen in Figs. 2 and 3 the average slope, which the model prediction represents, is almost identical for the resting and constricted condition and only differs in the dilated condition. Consequently E_p and β are very similar in the resting and constricted condition and is only markedly higher in the dilated condition, see Table 5. Therefore, if only the resting and constricted condition are used to evaluate the effect of smooth muscle activity on arterial stiffness, no difference can be observed based on E_p and β. Similarly, if one evaluates the pressure change-in-diameter behavior no difference can be observed since the curves collapse on each other. These stiffness quantities, however, completely ignore the shift of the pressure-radius loops toward lower, in case of smooth muscle contraction, and higher radii, in case of relaxation. This highlights their inability to truly quantify arterial stiffness and the need for new alternatives, possibly based on continuum-based mechanical models such as the one used herein.

The choice to combine the passive mechanical model from Gade et al. (2019) with a variant of the active model from Rachev and Hayashi (1999) is based on their simplicity and the low amount of model parameters which need to be

identified. Furthermore, the *in vivo* parameter identification method in Gade et al. (2019) has been (numerically) validated using a large data set.

The major difference between the passive mechanical model in Gade et al. (2019) and the ones used in other parameter identification methods (Masson et al. 2008; Spronck et al. 2015; Smoljkić et al. 2015; Heusinkveld et al. 2018) is the treatment of an artery as a thin-walled rather than a thick-walled structure. Although the geometry of an artery clearly resembles a thick-walled structure (Holzapfel et al. 2000), the existence of residual stress homogenizes the stress/stretch through the thickness (Takamizawa and Hayashi 1987; Fung 1991). This is further enhanced by smooth muscle activity (Rachev and Hayashi 1999; Humphrey and Wilson 2003) and results in an almost constant stress field throughout the arterial wall which is assumed in a thin-walled tube. Hence, the thin-walled assumption reproduces the arterial stress field to a high degree while allowing for easy analytical calculation of the gradient and Hessian of the objective function (15) which is beneficial for the parameter identification.

Another limitation is the assumption that an artery is only subjected to the blood pressure from within the lumen and prestretched in the axial direction. The *in vivo* loading situation is, however, more complex since an artery is constrained in its radial direction by surrounding tissue, organs, and bones (Humphrey 2002). This constraint is commonly incorporated by applying a perivascular pressure to the outside of an artery (Masson et al. 2008; Wittek et al. 2016). The perivascular pressure, which is reported to range from $0.67 - 0.93$ kPa in a normal population (De Keulenaer et al. 2009), reduces the transmural pressure and, therefore, decreases the stress state that the arterial wall experiences. Although it is trivial to extend the used arterial model to account for perivascular pressure, because P in Eqs. (1) and (2) represents the transmural pressure, the outside of an artery is assumed to be traction free and as a consequence arterial stiffness is slightly overestimated. This assumption is done to avoid using population averaged data for the individual person, if it is not essential. Furthermore, perivascular pressure depends on the blood pressure (Humphrey and Na 2002) and hence differs between the three arterial conditions: it is largest in the dilated condition and smallest in the constricted condition[3].

More advanced models to account for smooth muscle activity have been proposed and used to study the active behavior of arteries (Zulliger et al. 2004; Kroon 2009;

---

[3] The perivascular pressure might be close to zero or even negative during lower-body negative pressure because the pressure-radius measurements are performed in the vicinity of the pressure chamber, see Sect. 4.

Murtada et al. 2012; Stålhand et al. 2011; Schmitz and Böl 2011). These models consider the complete time evolution of the smooth muscle contraction, but from an *in vivo* parameter identification point of view, it is primarily the contracted state which is of importance. The active model in Rachev and Hayashi (1999) captures the intrinsic characteristics of smooth muscle contraction and requires only one additional parameter to be identified and was thus used herein.

Fitting the mechanical model to multiple pressure-radius loops simultaneously is a multi-objective minimization problem where each pressure-radius loop has its own objective. The multi-objective problem is reduced to a single-objective problem by summing up the individual objectives. There are two important aspects when solving this single-objective minimization problem: first, the functional form of the individual objectives; and second, the weighting of each individual objective.

Regarding the functional form of the individual objectives, an alternative to Eq. (14) could be:

$$\sum_{j=1}^{n} \left\{ w_{q1} \left[P^{\mathrm{mod}}(\boldsymbol{\kappa}, S_q, r_{\mathrm{i},qj}) - P_{qj} \right]^2 + \right.$$
$$\left. w_{q2} \left[F_{\mathrm{red}}^{\mathrm{mod}}(\boldsymbol{\kappa}, S_q, r_{\mathrm{i},qj}) - \bar{F}_{\mathrm{red}} \right]^2 \right\}, \tag{23}$$

where P^{mod} and $F_{\mathrm{red}}^{\mathrm{mod}}$ are given by Eqs. (20) and (21). We tried using this objective, but the determination of appropriate weights w_{11} and w_{12} is very challenging[4]. The simplest choice is to use $w_{q2} = 0$ and therefore neglect the behavior of the model in the axial direction. The problem then becomes overparameterized, however, because the parameters λ_z and β require some information about the axial direction. Even if a unique solution would be obtained by specifying one of those two parameters, e.g., by using population-averaged data, the behavior of the arterial model in the axial direction would still be unphysiological in terms of the magnitude of the reduced axial force and its variance throughout the cardiac cycle. The axial response of the arterial model must therefore be controlled in some way, preferably by the *in vitro* observation that the reduced axial force is approximately constant throughout the cardiac cycle (Van Loon et al. 1977; Weizsäcker et al. 1983) which we use.

The two parts in Eq. (23) do not describe analogous quantities and their relative magnitude to each other can vary substantially. Even if the first part of Eq. (23) is normalized by dividing it by P_{qj} and the second part by $\bar{F}_{\mathrm{red}}$, the selection of appropriate weighting factors is not trivial. By converting the pressure and reduced axial force into corresponding circumferential and axial stresses using the

equilibrium Eqs. (1) and (2), both parts of the individual objective represent analogous quantities and one receives an implicit normalization since both stresses have a similar magnitude. Furthermore, the choice for appropriate weighting factors appears more natural if both parts should equally contribute, cf. $w_1 = 0.5$ in Sect. 3.

In order to weigh each individual objective equally within the parameter identification problem ($\mathbb{P}$), they are normalized using their respective best-case and worst-case values, i.e., Utopia and Nadir points. In this study the Utopia and the Nadir points are calculated neglecting smooth muscle activity, i.e., only using the passive part of the mechanical model, and by using an estimate of the reduced axial force of 1 N. If the Utopia point is calculated with the complete mechanical model instead, its value is marginally smaller, at most 2% for both subjects. The corresponding minimization problem is, however, overparameterized and it is not straightforward to select the argument of the Utopia point in order to calculate the Nadir point. Other possibilities such as using the argument of the Utopia point and identifying an individual smooth muscle activity and reduced axial force for the determination of the Nadir point or normalizing by simply dividing ε_q by its Utopia point have been tested but the presented normalization scheme provided the best results. The well-working normalization scheme can be appreciated by examining Figures 2 and 3, and by comparing the coefficients of determination in Table 3 which barely deteriorated by fitting the model to multiple pressure-radius loops.

7 Conclusion

In this study, an *in vivo* parameter identification method for arteries is extended to account for smooth muscle activity. To overcome the problem of overparameterization due to an increased number of model parameters, the continuum-mechanical model is calibrated using data measured at multiple levels of vascular tone. Despite the simplicity of the mechanical model, it fits the measured pressure-radius loops at rest, under lower-body negative pressure and during physical exercise well.

Declarations

Conflict of interest The authors declare no potential conflict of interests.

---

[4] The choice of the weighting factors for the constricted and dilated arterial condition is trivial since only the pressure part is used.

References

Åstrand H, Rydén-Ahlgren Å, Sandgren T, Länne T (2005) Age-related increase in wall stress of the human abdominal aorta: an in vivo study. J Vasc Surg 42(5):926–31. https://doi.org/10.1016/j.jvs.2005.07.010

Åstrand H, Stålhand J, Karlsson J, Karlsson M, Sonesson B, Länne T (2011) In Vivo Estimation of the Contribution of Elastin and Collagen to the Mechanical Properties in the Human Abdominal Aorta: Effect of Age and Sex. J Appl Physiol 110(1):176–187. https://doi.org/10.1152/japplphysiol.00579.2010

Atkinson CL, Carter HH, Naylor LH, Dawson EA, Marusic P, Hering D, Schlaich MP, Thijssen DH, Green DJ (2015) Opposing effects of shear-mediated dilation and myogenic constriction on artery diameter in response to handgrip exercise in humans. J Appl Physiol 119(8):858–864. https://doi.org/10.1152/japplphysiol.01086.2014

Boutouyrie PH, Lacolley P, Briet M, Regnault V, Stéanton A, Laurent S, Mahmud A (2011) Pharmacological modulation of arterial stiffness. Drugs 71(13):1689–1701. https://doi.org/10.2165/11593790-000000000-00000

Bramwell JC, Hill AV (1922) The Velocity of the Pulse Wave in Man. Proc R Soc B Biol Sci 93(652):298–306. https://doi.org/10.1098/rspb.1922.0022

Cox RH (1978) Regional Variation of Series Elasticity in Canine Arterial Smooth Muscles. Am J Physiol 234(18):H542–H551. https://doi.org/10.1152/ajpheart.1978.234.5.h542

Cox RH, Jones AW, Swain ML (1976) Mechanics and electrolyte composition of arterial smooth muscle in developing dogs. Am J Physiol 231(1):77–83. https://doi.org/10.1152/ajplegacy.1976.231.1.77

Curry SJ, Krist AH, Owens DK, Barry MJ, Caughey AB, Davidson KW, Doubeni CA, Epling JW, Kemper AR, Kubik M, Landefeld CS, Mangione CM, Silverstein M, Simon MA, Tseng CW, Wong JB (2018) Risk assessment for cardiovascular disease with nontraditional risk factors: US preventive services task force recommendation statement. JAMA - J Am Med Assoc 320(3):272–280. https://doi.org/10.1001/jama.2018.8359

De Keulenaer BL, De Waele JJ, Powell B, Malbrain ML (2009) What is normal intra-abdominal pressure and how is it affected by positioning, body mass and positive end-expiratory pressure? Intensive Care Med 35(6):969–976. https://doi.org/10.1007/s00134-009-1445-0

Dobrin PB (1973) Influence of initial length on length tension relationship of vascular smooth muscle. Am J Physiol 225(3):664–670. https://doi.org/10.1152/ajplegacy.1973.225.3.664

Dobrin PB (1978) Mechanical properties of arteries. Physiol Rev 58(2):397–460. https://doi.org/10.1152/physrev.1978.58.2.397

Dobrin PB (2011) Vascular Mechanics. Compr. Physiol. American Cancer Society, chap 3:65–102. https://doi.org/10.1002/cphy.cp020303

Ferruzzi J, Vorp DA, Humphrey JD (2011) On Constitutive Descriptors of the Biaxial Mechanical Behaviour of Human Abdominal Aorta and Aneurysms. J R Soc Interface 8(56):435–450. https://doi.org/10.1098/rsif.2010.0299

Fridez P, Makino A, Kakoi D, Miyazaki H, Meister JJ, Hayashi K, Stergiopulos N (2002) Adaptation of conduit artery vascular smooth muscle tone to induced hypertension. Ann Biomed Eng 30(7):905–916. https://doi.org/10.1114/1.1507326

Fung YC (1991) What are the residual stresses doing in our blood vessels? Ann Biomed Eng 19(3):237–249. https://doi.org/10.1007/BF02584301

Gade JL, Stålhand J, Thore CJ (2019) An in vivo parameter identification method for arteries: numerical validation for the human abdominal aorta. Comput Methods Biomech Biomed Engin 22(4):426–441. https://doi.org/10.1080/10255842.2018.1561878

Green DJ, Hopman MT, Padilla J, Laughlin MH, Thijssen DH (2017) Vascular adaptation to exercise in humans: Role of hemodynamic stimuli. Physiol Rev 97(2):495–528. https://doi.org/10.1152/physrev.00014.2016

Heusinkveld MH, Quicken S, Holtackers RJ, Huberts W, Reesink KD, Delhaas T, Spronck B (2018) Uncertainty quantification and sensitivity analysis of an arterial wall mechanics model for evaluation of vascular drug therapies. Biomech Model Mechanobiol 17(1):55–69. https://doi.org/10.1007/s10237-017-0944-0

Hill AV (1938) The heat of shortening and the dynamic constants of muscle. Proc R Soc London Ser B - Biol Sci 126(843):136–195. https://doi.org/10.1098/rspb.1938.0050

Holzapfel GA, Gasser TC, Ogden RW (2000) A New Constitutive Framework for Arterial Wall Mechanics and a Comperative Study of Material Models. J Elast 61(1):1–48. https://doi.org/10.1023/A:1010835316564

Holzapfel GA, Sommer G, Auer M, Regitnig P, Ogden RW (2007) Layer-Specific 3D Residual Deformations of Human Aortas with Non-Atherosclerotic Intimal Thickening. Ann Biomed Eng 35(4):530–545. https://doi.org/10.1007/s10439-006-9252-z

Horný L, Adámek T, Gultova E, Zitny R, Vesely J, Chlup H, Konvickova S (2011) Correlations Between Age, Prestrain, Diameter and Atherosclerosis in the Male Abdominal Aorta. J Mech Behav Biomed Mater 4(8):2128–2132. https://doi.org/10.1016/j.jmbbm.2011.07.011

Horný L, Netušil M, Daniel M (2014) Limiting Extensibility Constitutive Model with Distributed Fibre Orientations and Ageing of Abdominal Aorta. J Mech Behav Biomed Mater 38:39–51. https://doi.org/10.1016/j.jmbbm.2014.05.021

Humphrey JD (2002) Cardiovascular Solid Mechanics, 1st edn. Springer-Verlag, New York. https://doi.org/10.1007/978-0-387-21576-1

Humphrey JD, Na S (2002) Elastodynamics and arterial wall stress. Ann Biomed Eng 30(4):509–523. https://doi.org/10.1114/1.1467676

Humphrey JD, Wilson E (2003) A potential role of smooth muscle tone in early hypertension: A theoretical study. J Biomech 36(11):1595–1601. https://doi.org/10.1016/S0021-9290(03)00178-7

Kawasaki T, Sasayama S, Yagi SI, Asakawa T, Hirai T (1987) Non-Invasive Assessment of the Age Related Changes in Stiffness of Major Branches of the Human Arteries. Cardiovasc Res 21(9):678–687. https://doi.org/10.1093/cvrese/21.9.678

Kroon M (2009) A constitutive model for smooth muscle including active tone and passive viscoelastic behaviour. Math Med Biol 27(2):129–155. https://doi.org/10.1093/imammb/dqp017

Laurent S, Alivon M, Beaussier H, Boutouyrie P (2012) Aortic stiffness as a tissue biomarker for predicting future cardiovascular events in asymptomatic hypertensive subjects. Ann Med 44(SUPPL. 1):S93–S97. https://doi.org/10.3109/07853890.2011.653398

MacDougall JD (1994) Blood Pressure Responses to Resistive, Static, and Dynamic Exercise. In: Fletcher GF (ed) Cardiovasc. Response to Exerc., chap 9. Futura Pub. Co, pp 155–173

Masson I, Boutouyrie PH, Laurent S, Humphrey JD, Zidi M (2008) Characterization of Arterial Wall Mechanical Behavior and Stresses from Human Clinical Data. J Biomech 41(12):2618–2627. https://doi.org/10.1016/j.jbiomech.2008.06.022

Matsumoto T, Hayashi K (1996) Stress and Strain Distribution in Hypertensive and Normotensive Rat Aorta Considering Residual Strain. J Biomech Eng 118(1):62–73

Mausser H (2006) Normalization and Other Topics in Multi-Objective Optimization. In: Proceeding Fields-MITACS Ind. Probl. Work., pp 89–101

Mozaffarian D, Benjamin EJ, Go AS, Arnett DK, Blaha MJ, Cushman M, Das SR, de Ferranti S, Després JP, Fullerton HJ, Howard VJ, Huffman MD, Isasi CR, Jiménez MC, Judd SE, Kissela BM, Lichtman JH, Lisabeth LD, Liu S, Mackey RH, Magid DJ, McGuire DK, Mohler ER, Moy CS, Muntner P, Mussolino ME, Nasir K, Neumar RW, Nichol G, Palaniappan L, Pandey DK, Reeves MJ, Rodriguez CJ, Rosamond W, Sorlie PD, Stein J, Towfighi A, Turan TN, Virani SS, Woo D, Yeh RW, Turner MB (2016) Heart Disease and Stroke Statistics – 2016 Update: A Report From the American Heart Association, vol 133. doi: https://doi.org/10.1161/cir.0000000000000350

Murtada SI, Arner A, Holzapfel GA (2012) Experiments and mechanochemical modeling of smooth muscle contraction: Significance of filament overlap. J Theor Biol 297:176–186. https://doi.org/10.1016/j.jtbi.2011.11.012

Nash JE, Sutcliffe JV (1970) River flow forecasting through conceptual models part I - A discussion of principles. J Hydrol 10:282–290. https://doi.org/10.1016/0022-1694(70)90255-6

Nocedal J, Wright SJ (1999) Numerical Optimization, 2nd edn. Springer, New York. https://doi.org/10.1002/lsm.21040

Peterson LH, Jensen RE, Parnell J (1960) Mechanical Properties of Arteries in Vivo. Circ Res 8(3):622–639. https://doi.org/10.1161/01.RES.8.3.622

Price JM, Davis DL, Knauss EB (1981) Length-dependent sensitivity in vascular smooth muscle. Am J Physiol - Hear Circ Physiol 10(4):557–563. https://doi.org/10.1152/ajpheart.1981.241.4.h557

Rachev A, Hayashi K (1999) Theoretical Study of the Effects of Vascular Smooth Muscle Contraction on Strain and Stress Distributions in Arteries. Ann Biomed Eng 27(4):459–468. https://doi.org/10.1114/1.191

Reesink KD, Spronck B (2019) Constitutive interpretation of arterial stiffness in clinical studies: A methodological review. Am J Physiol - Hear Circ Physiol 316(3):H693–H709. https://doi.org/10.1152/ajpheart.00388.2018

Rhodin JAG (2014) Architecture of the Vessel Wall. In: Compr. Physiol., American Cancer Society, chap 1, pp 1–31, doi: https://doi.org/10.1002/cphy.cp020201

Roach MR, Burton AC (1957) The Reason for the Shape of the Distensibility Curves of Arteries. Can J Biochem Physiol 35(8):681–690. https://doi.org/10.1139/o57-080

Schmitz A, Böl M (2011) On a phenomenological model for active smooth muscle contraction. J Biomech 44(11):2090–2095. https://doi.org/10.1016/j.jbiomech.2011.05.020

Schriefl AJ, Zeindlinger G, Pierce DM, Regitnig P, Holzapfel GA (2012) Determination of the layer-specific distributed collagen fibre orientations in human thoracic and abdominal aortas and common iliac arteries. J R Soc Interface 9(71):1275–1286. https://doi.org/10.1098/rsif.2011.0727

Schulze-Bauer CAJ, Holzapfel GA (2003) Determination of Constitutive Equations for Human Arteries from Clinical Data. J Biomech 36(2):165–169

Schulze-Bauer CAJ, Mörth C, Holzapfel GA (2003) Passive Biaxial Mechanical Response of Aged Human Iliac Arteries. J Biomech Eng 125(3):395–406. https://doi.org/10.1115/1.1574331

Sehgel NL, Zhu Y, Sun Z, Trzeciakowski JP, Hong Z, Hunter WC, Vatner DE, Meininger GA, Vatner SF (2013) Increased vascular smooth muscle cell stiffness: A novel mechanism for aortic stiffness in hypertension. Am J Physiol - Hear Circ Physiol 305(9):1281–1287. https://doi.org/10.1152/ajpheart.00232.2013

Smoljkić M, Vander Sloten J, Segers P, Famaey N (2015) Non-Invasive, Energy-Based Assessment of Patient-Specific Material Properties of Arterial Tissue. Biomech Model Mechanobiol 14(5):1045–1056. https://doi.org/10.1007/s10237-015-0653-5

Somlyo AP, Somlyo AV (1992) Smooth Muscle Structure and Function. In: Fozzard HA (ed) Hear Cardiovasc Syst, 2nd edn. Raven Press Ltd, New York, pp 1295–1324

Sonesson B, Länne T, Vernersson E, Hansen F (1994) Sex Difference in the Mechanical Properties of the Abdominal Aorta in Human Beings. J Vasc Surg 20(6):959–969. https://doi.org/10.1016/0741-5214(94)90234-8

Sonesson B, Vernersson E, Hansen F, Länne T (1997) Influence of Sympathetic Stimulation on the Mechanical Properties of the Aorta in Humans. Acta Physiol Scand 159(2):139–145. https://doi.org/10.1046/j.1365-201X.1997.581343000.x

Spronck B, Heusinkveld MH, Donders WP, De Lepper AG, Roodt JO, Kroon AA, Delhaas T, Reesink KD (2015) A constitutive modeling interpretation of the relationship among carotid artery stiffness, blood pressure, and age in hypertensive subjects. Am J Physiol - Hear Circ Physiol 308(6):H568–H582. https://doi.org/10.1152/ajpheart.00290.2014

Stålhand J (2009) Determination of Human Arterial Wall Parameters from Clinical Data. Biomech Model Mechanobiol 8(2):141–148. https://doi.org/10.1007/s10237-008-0124-3

Stålhand J, Klarbring A (2005) Aorta In Vivo Parameter Identification Using an Axial Force Constraint. Biomech Model Mechanobiol 3(4):191–199. https://doi.org/10.1007/s10237-004-0057-4

Stålhand J, Klarbring A, Holzapfel GA (2011) A mechanochemical 3D continuum model for smooth muscle contraction under finite strains. J Theor Biol 268(1):120–130. https://doi.org/10.1016/j.jtbi.2010.10.008

Takamizawa K, Hayashi K (1987) Strain energy density function and uniform strain hypothesis for arterial mechanics. J Biomech 20(1):7–17. https://doi.org/10.1016/0021-9290(87)90262-4

Tortora GJ, Derrickson B (2012) Prinicples of anatomy & physiology, 13th edn. John Wiley & Sons Inc

Treloar LRG (1943) The elasticity of a network of long-chain molecules-II. Trans Faraday Soc 39:241–246. https://doi.org/10.1039/TF9433900241

Van Loon P, Klip W, Bradley EL (1977) Length-Force and Volume-Pressure Relationships of Arteries. Biorheology 14(4):181–201

Van Sloten TT, Schram MT, Van Den Hurk K, Dekker JM, Nijpels G, Henry RM, Stehouwer CD (2014) Local stiffness of the carotid and femoral artery is associated with incident cardiovascular events and all-cause mortality: The hoorn study. J Am Coll Cardiol 63(17):1739–1747. https://doi.org/10.1016/j.jacc.2013.12.041

Vlachopoulos C, Xaplanteris P, Aboyans V, Brodmann M, Cífková R, Cosentino F, De Carlo M, Gallino A, Landmesser U, Laurent S, Lekakis J, Mikhailidis DP, Naka KK, Protogerou AD, Rizzoni D, Schmidt-Trucksäss A, Van Bortel L, Weber T, Yamashina A, Zimlichman R, Boutouyrie P, Cockcroft J, O'Rourke M, Park JB, Schillaci G, Sillesen H, Townsend RR (2015) The role of vascular biomarkers for primary and secondary prevention. A position paper from the European Society of Cardiology Working Group on peripheral circulation. Endorsed Associat Res Arterial Struct Physiol (ARTERY. Atherosclerosis) 241(2):507–532. https://doi.org/10.1016/j.atherosclerosis.2015.05.007

Vukasovic J, Al-Timman J, Hainsworth R (1990) The effects of lower body negative pressure on baroreceptor responses in humans. Exp Physiol 75(1):81–93. https://doi.org/10.1113/expphysiol.1990.sp003388

Weizsäcker HW, Lambert H, Pascale K (1983) Analysis of the Passive Mechanical Properties of Rat Carotid Arteries. J Biomech 16(9):703–715. https://doi.org/10.1016/0021-9290(83)90080-5

White DD, Gotshall RW, Tucker A (1996) Women have lower tolerance to lower body negative pressure than men. J Appl Physiol 80(4):1138–1143. https://doi.org/10.1152/jappl.1996.80.4.1138

Wilkins E, Wilson L, Wickramasinghe K, Bhatnagar P, Leal J, Luengo-Fernandez R, Burns R, Rayner M, Townsend N (2017) European Cardiovascular Disease Statistics 2017. Eur Hear Network, Brussels p 192, doi: 978-2-9537898-1-2

Wittek A, Derwich W, Karatolios K, Fritzen P, Vogt S, Schmitz-Rixen T, Blase C (2016) A Finite Element Updating Approach for Identification of the Anisotropic Hyperelastic Properties of Normal and Diseased Aortic Walls from 4D Ultrasound Strain Imaging. J Mech Behav Biomed Mater 58:122–138. https://doi.org/10.1016/j.jmbbm.2015.09.022

Zieff GH, Heffernan K, Stone K, Fryer S, Credeur D, Hanson ED, Faulkner J, Stoner L, Article O (2019) The pressure-dependency of local measures of arterial stiffness. J Hypertens 37(5):956–963. https://doi.org/10.1097/HJH.0000000000001998

Zulliger MA, Rachev A, Stergiopulos N (2004) A constitutive formulation of arterial mechanics including vascular smooth muscle tone. Am J Physiol - Hear Circ Physiol 287(3 56–3):1335–1343. https://doi.org/10.1152/ajpheart.00094.2004